Optimal Positioning of Ground Base Stations in Free-Space Optical Communications for High-Speed Trains

Sina Fathi Kazerooni, Yagiz Kaymak, *Student Member, IEEE,* Roberto Rojas-Cessa, *Senior Member, IEEE,* Jianghua Feng, Nirwan Ansari, *Fellow, IEEE,* Mengchu Zhou, *Fellow, IEEE,* and Tairan Zhang

***Abstract*—In this paper, we propose two different free-space-optics (FSO) coverage models for high-speed-train (HST) communications. The models provide different coverage areas for performing seamless signal handover and uninterrupted ground-to-train communication. The first model uses two different wavelengths in adjacent covered areas and the second one uses a single wavelength. We find the optimal distance from the train track to a ground base station and the distance between base stations to provide seamless connectivity and handover while minimizing the number of base stations along the track. We base our estimations on a realistic model of an FSO system and provide numerical evaluations demonstrating the performance of the proposed coverage models. We show the different amounts of received power on ground-to-train communications as a function of the location of ground base stations. We also consider the effect of fog on the FSO link as the most attenuating condition for FSO communications. Our results show that using the optimal distance between adjacent base stations achieve communications of 1 Gpbs and higher rates.**

***Index Terms*—Free-space optical communications, High-speed trains, Laser-based optical links, Optimal base station location, Beam coverage, FSO**

I. Introduction

HIGH-SPEED trains (HSTs) traveling at speeds faster than 250 km/h are globally becoming the choice of transportation for a large number of long-distance commuters. Some of the fastest trains have a maximum operational speed of 430 km/h [1]. The increasing adoption rate of public high-speed transportation systems and the number of Internet connected digital devices pose a large demand for fast and reliable Internet access in trains, as reportedly occurring in the city of Chicago [2].

Providing high-speed Internet access in HSTs poses multiple challenges. Performing seamless and efficient handovers as the train moves is one of the main challenges. Current available technologies, such as Long Term Evolution (LTE) of the 3rd Generation Partnership Project (3GPP), WiMAX, and other radio-frequency based systems suffer from frequent and unreliable handovers [3]–[6]. Doppler frequency shifts and penetration losses in environments with high-speed mobility affect handovers in communications for HSTs [7]–[9]. The increased speed of HSTs poses concerns in terms of train operation safety [10]. Communication-based train control (CBTC) uses bidirectional ground-to-train communications to provide automated train control system [11]. CBTC systems use IEEE 802.11p [12] as the communication platform. However, IEEE 802.11p suffer from similar shortcomings that the other radio-frequency systems for HSTs do.

Conventional radio-frequency-based handover mechanisms, such as those adopted in LTE, are triggered by the amount of received signal strength (RSS) from neighboring eNodeB (eNB) cells [13]. If the RSS of a neighboring cell becomes larger than that of the serving cell for at least a duration equal to the time-to-trigger period, the user equipment sends the RSS measurement to the serving eNB, which in turn sends a handover request back to the UE. After that, a handover process is executed [14]. During this time, the UE stops communicating with the serving eNB before connecting to the (new) target eNB, and thus, generating communication interruptions.

Previous works in radio frequency systems have proposed using dual antennas on trains to reduce interruptions during handover [15], [16]. These advanced LTE systems are currently capable of providing a 100-Mbps connection [9]. WiMAX systems are reported capable of providing up to 75-Mbps data rates but the actual operating rates are less than 1 Mbps in high-speed mobile systems [17].

Communications for HSTs must be capable of providing high data-rate connections for high-definition (HD) video transmissions such as video streaming, surveillance videos, real-time conferencing, and real-time train motion video used for driverless train systems [18]. As an example of an estimated user data demand, real-time HD video streaming from Netflix requires data rates of 5 Mbps per user [19]. In an HST with 180 passengers, if 20% of the passengers stream HD video at the same time, they would need a 180-Mbps data rate, which cannot be satisfied with a current 20-MHz 64-QAM LTE connection bandwidth [20] (whose rate limit is 100.8 Mbps [9]). Therefore, with the growing demand for streaming services and real-time video requirements for HSTs' maintenance and operation, the future communication requirements for HSTs calls for large-bandwidth connectivity.

Free-space optics (FSO) based on laser light is a recent technology for providing HST communications. This tech-

S. Fathi Kazerooni, Y. Kaymak, R. Rojas-Cessa, N. Ansari, and M. Zhou are with Department of Electrical and Computer Engineering, New Jersey Institute of Technology, Newark, NJ 07102. Email: {sina.fathi.kazerooni,yk79, rojas, ansari, zhou}@njit.edu.

J. Feng and T. Zhang are with CRRC Zhuzhou Institute Co., LtD, Shidai Road, Zhuzhou, Hunan Province, China Email: {fengjh, zhangtrg}@csrzic.com. This work is supported in part by CRRC Zhuzhou Institute Co., Ltd.

nology is already adopted for providing point-to-point data communications in stationary places, in lieu of cable or optical fiber [21], [22]. Current data rates of operational FSO systems are up to 100 Gbps and prototype systems are reported with a capacity of 400 Gbps per channel for a total capacity of 20 Tbps [23].

The channel capacity of FSO communications systems for HSTs may be smaller than it is for stationary point-to-point FSO systems because of the high-speed mobility of the train. Yet, an FSO system could potentially provide high-bandwidth connections for HSTs. However, a major challenge is handover delay, as this delay may impede achieving uninterrupted transmission of data during the handover time [24], [25].

A recently proposed handover mechanism for FSO systems stops communications during the handover process, generating an interruption period [25]. Another factor that may prolong the handover delay is the tracking mechanism of a mobile FSO communications system [25]. This tracking system is used to orientate the train transceivers and continuously track the laser beam of the ground base station (or base station for short) to which the train is connected by employing fast steering mirrors. In this system, the train transceiver incorporates a complementary metal oxide semiconductor (CMOS) sensor to find and track each base station along the track. As the train travels along the track, the CMOS sensor detects the beacon light emitted by the next base station. At this time, the train transceiver disconnects from the current base station and starts the handover process to the next. A seamless connection at the application layer is claimed possible in this system, if the handover time is very short [25].

There are several existing analytical studies on FSO communications for trains involving geometrical models [26]–[28], but they neglect the impact of the handover time on achievable data rates. The currently known FSO model for HSTs [25] has a coverage distance along the track where the train gets in contact with the base station and handover is performed. After a successful handover, a ground-to-train communications link is established. Another geometrical model of Ricean fading channel but for vehicle-to-vehicle communication derives the level crossing rate (LCR) and average fade duration (AFD) for radio frequency systems [29], [30].

For the FSO system to be efficient, the time to complete a handover must be shorter or equal to the communication time (i.e., the time in which the train and base station exchange users' data). To achieve that, we propose two FSO coverage models which can provide seamless handovers and high-bandwidth communications for HSTs.

Our proposed coverage models differ in the number of wavelengths used in ground-to-train HST communications and the extent of the coverage distance. This distance is a segment of the track that the train moves along within the beam's coverage area. In both models, the train is permanently connected to base stations and handovers are seamlessly performed. These models do not use laser tracking systems because the laser beam is spread along the track and this beam provides sufficient received power at each point along the track for achieving a large bandwidth connection. These two models are: 1) the Dual Wavelength (DW) model, in which two different wavelengths are used alternately by adjacent base stations, and 2) the Single Wavelength (SW) model, in which every station use the same single wavelength.

In the DW model, the laser-light beams of two base stations overlap at the edges of their coverage distance, producing an overlapping coverage region along the track where handover takes place. An HST finds out the time to perform a handover by detecting a signal in a frequency different from the last one used. The HST must complete the handover while the train's transceiver travels through the overlapping region. The train uses one or more transceivers to maintain communication with the connected base station while the front transceiver completes the handover with the target station.

In the SW model, ground-station beams do not overlap on the train's path, leaving a segment of the track uncovered by the laser beams in between covered distances. We call this uncovered segment *dark region*. Therefore, the train also uses one or more transceivers to communicate with a base station during the handover time. The train may use the dark region to identify the time to initiate a handover. In this model, the length of the dark region, which is a function of the required time to perform a handover and the speed of the train, may be used to increase the separation distance between base stations.

We determine the optimal distance between base stations and the track to provide the minimum number of base stations along the track, the strongest received signal power, and the required contact time to make the FSO system efficient. Here, contact time is referred to as the time period in which train transceivers receive detectable laser beams, including the communication and the handover times.

Our analysis adopts a number of realistic and accepted loss models for FSO communications. Our approach aims to ensure an operational FSO link even in poor weather conditions, including heavy fog, rain, haze, etc. The proposed coverage models aim to attain links with high bandwidth through finding the optimal location of base stations.

We identify the optimal distance of a base station to both the track and its adjacent base station for providing efficient and uninterrupted HST communications. We base our calculations on both the minimum required received power by the transceivers placed on top of a train traveling at 400 km/h and the sensitivity threshold of the photodiodes used in FSO transceivers.

The remainder of this paper is organized as follows. Section II describes the DW model, which uses two alternating wavelengths. Section III introduces our SW model, which uses a single wavelength. Section IV presents numerical evaluations of performance of these two models and the optimal location of the base stations. Section V presents our conclusions.

II. Dual Wavelength Model

In this model, base stations use two different wavelengths for communicating with an HST. A base station uses one wavelength and the adjacent one uses the other wavelength, and so forth, alternatively. For example, one base station may use an 850-nm wavelength and the adjacent one may use a 1550-nm wavelength. Then, the following station may use an

850-nm wavelength, and so on. Figure 1 shows the lateral view of a train. In this figure, h represents the height of train transceivers and also the height of a ground base station from the ground.

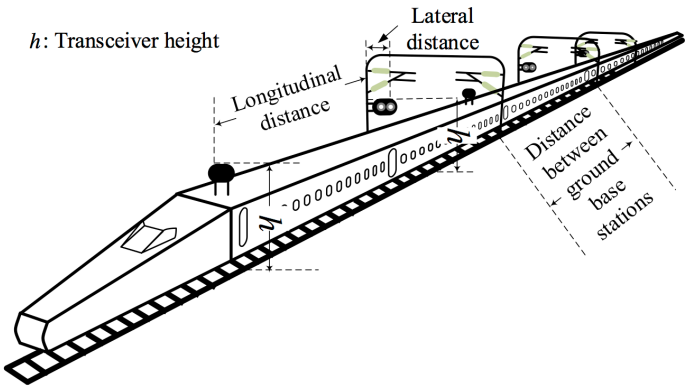

Fig. 1. Positioning of transceivers on train and base stations.

The coverage distance of base station B_i is defined between C_i and D_i, $|C_iD_i|$, as Figure 2 shows. In this model, the laser lights emitted by two consecutive base stations have an overlapping region. This figure also shows this overlapping region, $C_{i+1}D_i$, where C_{i+1} is the first point of the coverage distance of base station B_{i+1} and D_i is the farthest point of it. To achieve uninterrupted communications, the train uses two or more transceivers on the roof, each positioned at different distances from the front of the train. In this paper we base our models on using two transceivers but more transceivers may be used. For simplicity, we assume that the distance between the front and rear transceivers is equal to the length of overlapping region (herein, we consider that all overlapping regions have the same length). Alternating frequencies in this model trigger the start of a handover. When the front transceiver enters the overlapping region, it detects another laser light with a different wavelength from the one it is communicating with. Then, the train enables the rear transceiver to continue communicating with the current base station, while the front transceiver stops communicating with it and initiates a handover process with the next base station. During this handover period, the rear transceiver remains connected to the current base station and provides the users with a seamless Internet connection.

A. Placement of Base Stations

As shown in Figure 2, two adjacent base stations, B_i and B_{i+1}, share an overlapping region, $C_{i+1}D_i$. Base station B_{i-1} also shares an overlapping region, C_iD_{i-1}, with the previous base station, and so on. The overlapping region is the region where handover takes place as a train moves through it. The distance of the overlapping region is a function of the train speed and the time it takes to perform the handover. The connection region, $D_{i-1}D_i$, is the region where the train and the base station can exchange users' data. In the analysis presented in this paper, the laser beams of the base stations use the same divergence angle (θ) and coverage angle (δ).

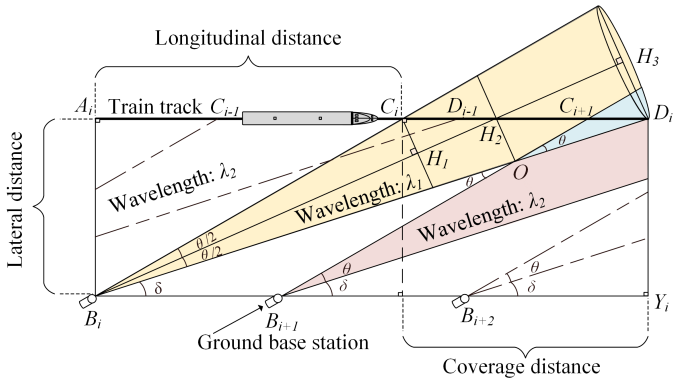

Fig. 2. Superior view of the DW model.

We calculate the coverage distance of a base station based on the target duty cycle of 2:1 (data communication time to handover time in a coverage distance) and the speed of the train. This duty cycle provides a balanced case scenario on handover time and communication time in our analysis. Moreover, it is the worst case scenario where the handover takes as much time as the connection time, therefore, making it inefficient. This coverage distance is then used to calculate the lateral and longitudinal distances of a base station. The lateral and longitudinal distances of base station B_i from A_i are the perpendicular distance of B_i from the track, $|B_iA_i|$ and the distance of the beginning of the coverage distance from the projection of B_i on the track axis, $|C_iA_i|$, respectively. Figure 2 shows the distance between base stations, $|B_iB_{i+1}|$, and the distances of the overlapping regions, $|C_iD_{i-1}|$ and $|C_{i+1}D_i|$, where handovers are performed.

For example, the coverage distance for a train traveling at a constant velocity of 400 km/h (or 111.11 m/s) and with a connection time set to twice as long as the handover duration is then 333.33 m. This calculation considers the longest reported handover time in FSO systems for HSTs of 1 s [31]. The distance between transceivers required to provide seamless connectivity is equal to the handover distance. For a train with only two transceivers, the minimum train length is then the handover distance. For a shorter train, a disconnection may occur, and the disconnection time is calculated as: $t_d = \frac{|C_{i+1}D_i|-d}{s}$, where t_d is the duration of disconnection, d is the distance between train transceivers, and s is the speed of the train. Nevertheless, the disconnection time can be avoided by considering the length of the shortest expected train by the train operator. The train uses at least one additional transceiver to communicate with a base station during the handover time. In this example, if the train's length is longer than 400 m, we may use more than two train transceivers.

The divergence and coverage angles are determined as follows [26]:

$$\theta = \arctan \frac{|B_iA_i|\,|C_iD_i|}{|B_iA_i|^2 + |C_iA_i|^2 + |C_iA_i| \times |C_iD_i|} \tag{1}$$

$$\delta = \arctan \frac{|B_iA_i|}{|A_iD_i|} \tag{2}$$

The distance between two neighboring base stations is:

$$\begin{aligned} |B_iB_{i+1}| &= |C_iD_i| - |C_{i+1}D_i| \\ &= |C_iC_{i+1}| \end{aligned} \tag{3}$$

The laser beam is modeled as a Gaussian beam [32] in this paper. To calculate the received power at a point along the coverage distance, first, we calculate the optical beam offset and radius. The optical beam offset, r, from the axis of propagation is equal to the perpendicular line to the axis of propagation drawn at the point of interest along the coverage distance. The optical beam radius, w, is equal to the distance from the image of the point of interest along the coverage distance on the axis of propagation to either one of the boundaries of the beam.

In this paper, we define x as the distance from the first coverage point (i.e., C_i) to a point where the beam radius and the beam offset from the propagation axis are calculated. The beam offset is calculated as:

$$r = ||C_iH_2| - x| \sin(\frac{\theta}{2} + \delta) \tag{4}$$

The beam radius, w, is calculated as [32]:

$$w = w_0 \left[1 + \left(\frac{\lambda z}{\pi w_0^2}\right)^2\right]^{0.5} \tag{5}$$

where w_0 is the beam waist at source and z is the distance along the axis of propagation. Considering the Rayleigh normalization, w increases linearly with z at large distances [33]. Therefore, we calculate w as:

$$w = (|B_iH_2| - (|C_iH_2| - x)\cos(\frac{\theta}{2} + \delta)) \tan\frac{\theta}{2} \tag{6}$$

where H_2 is the intersection of the axis of propagation and the coverage distance.

At point C_i, optical beam offset and beam radius are equal. The beam radius at this point is:

$$|C_iH_1| = |B_iC_i| \sin\frac{\theta}{2} \tag{7}$$

The optical beam radius is zero at H_2 and the received power is the largest in comparison with the other points in the coverage distance. The beam radius at H_2 is:

$$|OH_2| = |B_iO| \sin\frac{\theta}{2} \tag{8}$$

The optical beam offset, $|D_iH_3|$, is equal to the beam radius from the axis of propagation (i.e., B_iH_3) at the farthest point of the coverage distance along the track [32]. The calculation of the beam radius at this point, $|D_iH_3|$, in the triangle $\triangle B_iH_3D_i$, follows the Law of Sines:

$$|B_iD_i| = \frac{|Y_iD_i|}{\sin\delta} = \frac{|B_iA_i|}{\sin\delta} \tag{9}$$

$$|D_iH_3| = |B_iD_i| \sin\frac{\theta}{2} \tag{10}$$

It then remains to calculate the received power at the train transceivers.

B. Calculation of Received Power

The calculation of the received power (P_r) along the axis of propagation, B_iH_3, uses Friis equation, which is a function of the transmitted power and different system losses [23]:

$$\frac{P_r}{P_t} = G_tG_r\left(\frac{\lambda}{4\pi R}\right)^2 L_{geo}L_tL_r\eta_r\eta_t \tag{11}$$

Here, L_t and L_r are the transmitter and receiver pointing losses, respectively. These losses are calculated as:

$$L_t = e^{-G_t\gamma^2} \tag{12}$$

where γ is the angle of transmitter radial pointing error [34], in radians, and

$$L_r = e^{-G_r\zeta^2} \tag{13}$$

where ζ is the angle of receiver radial pointing error, G_r and G_t are the receiver and transmitter system gains, respectively, η_r and η_t are optical efficiencies at the receiver and transmitter, respectively, and L_{geo} is the geometrical loss of the laser beam. The calculation of G_t for a Gaussian beam follows [35]:

$$G_t = \frac{32}{\theta^2} \tag{14}$$

where θ is in radians. The receiver antenna gain (G_r) is calculated as [23], [36]:

$$G_r = \left(\frac{\pi D_r}{\lambda}\right)^2 \tag{15}$$

where D_r is the telescope aperture diameter (antenna size).

The light emitted by laser LEDs disperses conically and causes loss of power at different cross-sections of the light, which is calculated as [37]:

$$L_{geo} = \frac{S_r}{S_t + {}^{\pi}/_{4}(\theta R)^2} \tag{16}$$

where S_r and S_t are the surface areas of the receiver and transmitter, respectively. In (16), R is the link range (i.e., the total distance from the base station to the transceiver on the train), in meters.

The calculation of the loss of power caused by atmospheric conditions, such as fog or rain uses Kruse [38] model, which is based on Beers-Lambert's Law [39]. The power loss is calculated as:

$$L_a = \frac{17}{V}\left(\frac{\lambda}{550 \text{ nm}}\right)^{-q} \tag{17}$$

where L_a is in dB/km, V is the visibility in km, λ is the wavelength of the laser light in nm, and q is the size distribution of the scattering particles. Scattering particles include air molecules, haze particles, fog droplets, rain, snow, and hail. These particles have different scattering strength. Therefore, they have different attenuation effects on FSO communications. Depending on the weather condition, q may have different values, as listed below [40]:

$$q = \begin{cases} 1.6 & \text{for high visibility } (V > 50 \text{ km}) \\ 1.3 & \text{for average visibility } (6 \text{ km} < V < 50 \text{ km}) \\ 0.16\,V + 0.34 & \text{for haze visibility } (1 \text{ km} < V < 6 \text{ km}) \\ V - 0.5 & \text{for mist visibility } (0.5 \text{ km} < V < 1 \text{ km}) \\ 0 & \text{for fog visibility } (V < 0.5 \text{ km}) \end{cases}$$

The calculation of the received power along the axis of the propagation, P_0, considering the attenuation caused by weather conditions, is as follows:

$$P_0(R) = 10\log(P_r) - L_a R \tag{18}$$

where P_0 is in dBm. To calculate the received power at each point along the track, we use the fundamental mode of a Gaussian beam, which follows a Gaussian distribution of the electric field perpendicular to the propagation axis [32]. The relationship between the received power along the axis of propagation and a point along the track with radius w from the axis of propagation is given as [32]:

$$\frac{P_{rx}(r,R)}{P_0(R)} = \exp\left[-2\Big(\frac{r}{w}\Big)^2\right] \tag{19}$$

where $P_{rx}(r,R)$ is the received power at a point with beam offset r from the propagation axis. Note that (19) is also known as edge taper [32].

C. Problem Formulation

We describe the objective of finding the optimal longitudinal and lateral distances as the following optimization problem:

$$\begin{aligned}
\underset{|C_iA_i|,|B_iA_i|}{\text{maximize}} \quad & P_{rx}(r,R) \\
\text{subject to} \quad & P_{rx}(w,R) \geq S_r, \\
& P_t = P_{const}, \\
& |C_iD_i| = d_{cvrd}, \\
& |B_iA_i| > |B_iA_i|_{min}, \\
& |C_iA_i| > 0, \\
& \theta > 0, \\
& \delta > 0.
\end{aligned}$$

where S_r is the *receiver sensitivity* or the minimum required received power to detect the laser beam [41], P_{const} is the limited and constant transmitting power at source, and d_{cvrd} is the given covered distance, and $|B_iA_i|_{min}$ is the smallest lateral distance to the track at which a base station may be placed.

III. Single Wavelength Model

In this section, we introduce the SW model for providing extended FSO coverage in HST communications. Base stations in this model are set to use a laser light using a single wavelength (e.g., a 1550-nm wavelength).

A. Model Description

In this model, the coverage distances of the laser beams are separated along the track and thus form a dark region, instead of an overlapping region as in the DW model. The dark region may also function as the trigger to start a handover process. Figure 3 shows the SW model.

When entering a dark region, the train's front transceiver stops communicating with the last base station while the rear transceiver continues communicating with it. The front transceiver starts a handover process with the next base station when it enters the area covered by that base station. The handover process is completed by the time the rear transceiver of the train reaches the dark region. Seamless handover is then achieved by having a transceiver connected all the time.

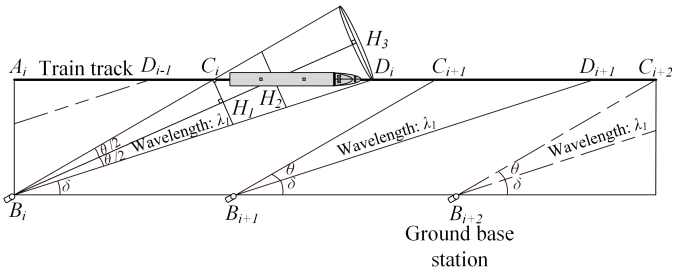

Fig. 3. Superior view of the SW model.

In general, the notations used in the SW model follow the ones used in the DW model. However, $|D_iC_{i+1}|$ in the SW model represents the dark region along the track, as Figure 3 shows.

The length of the dark region increases the distance between base stations (and reduces the number of base stations), and therefore, the SW model minimizes the cost of the FSO system in comparison with the DW model. The distance between the front and rear transceivers of a train equals the length of the dark region plus the distance needed for a successful handover. The length of a dark region, L_D, is estimated as:

$$L_D = d_{trans} - vt \tag{20}$$

where v is the velocity of the train, t is the time it takes the train to complete the handover, and d_{trans} is the distance between two consecutive train transceivers. Therefore, vt is the distance that the train travels during a handover period. As (20) indicates, d_{trans} must be larger than or equal to vt and also smaller than the coverage distance of a base station for a seamless handover. Figure 3 shows L_D as $|D_iC_{i+1}|$. The distance between two consecutive base stations is:

$$|B_iB_{i+1}| = |C_iD_i| + L_D \tag{21}$$

As an example, for a train traveling at a speed of 400 km/h and with two transceivers separated 400 m, L_D is about 289 m by considering one second as the time to complete the handover successfully. Therefore, for the same longitudinal and lateral distances as in the DW model, the SW model allows increasing the distance between adjacent base stations. Table I summarizes the different distances used in the DW and SW models.

TABLE I
List of Variables

Variable	Definition
$\|B_iA_i\|$	Lateral distance
$\|A_iC_i\|$	Longitudinal distance
$\|B_iB_{i+1}\|$	Distance between two consecutive base stations
$\|C_iD_i\|$	Coverage distance of base station B_i
$\|C_{i+1}D_i\|$	Overlapping region distance in the DW model
$\|D_iC_{i+1}\|$	Dark region distance in the SW model

B. Calculation of the Received Power

The maximum achievable coverage distance of a base station for different longitudinal and lateral distances of a base station is a function of the receiver sensitivity. A transceiver placed at D_i along the track would receive the smallest amount of power. The estimation of the maximum coverage distance for which the received power is greater than the receiver sensitivity is based on this smallest amount of received power.

IV. Numerical Analysis Results

We performed numerical evaluations of the proposed models in MATLAB®. Table II lists the parameters and their values used in our simulations. In this table, L_{sys} corresponds to the combined system losses, L_t and L_r [36]. The results presented in this section consider heavy fog as the weather condition. This condition is considered as the worst-case scenario for realizing FSO communications. Under this weather condition, we estimate the optimal location of base stations in reference to the track to guarantee that our proposed models are capable of providing the train with a large-bandwidth communication channel. To achieve this objective, the received power of the signal by the transceivers must be larger than the receiver sensitivity. A typical receiver sensitivity for communicating at a rate of 1.25 Gbps with ON-OFF keying modulation is -36 dBm in Si and InGaAs avalanche photo detectors [42]. Antenna spacing on the train has been designed according to requirement of each model to provide seamless connectivity to the users. Antenna spacing may be changed by adding more antennas or changing the transmitting power or using a receiver with higher sensitivity. The detection of a signal on a different wavelength is used to trigger the start of the handover for the DW model and the detection of a signal after a dark region for the SW model. Therefore, the received power at triggering points must be more than receiver sensitivity.

TABLE II
Evaluation Parameters

Variable	Description	Value
λ_1	Laser light wavelength 1	1550 nm
λ_2	Laser light wavelength 2	850 nm
P_t	Transmitting power	27 dBm
S_{tx}	Surface area of transmitter	9 cm^2
S_{rx}	Surface area of receiver	95 cm^2
V	Visibility in fog conditions	0.5 km
η_t	Lens efficiency of transmitter	1
η_r	Lens efficiency of receiver	1
L_{sys}	System losses	0.5
v	Speed of the train	400 km/h
S_r	Receiver responsivity at 1.25 Gbps	-36 dBm

We calculate the required coverage distance of a base station using the DW model by considering one second as the largest handover time and a duty cycle of 2:1. In such a scenario, a train traveling at 400 km/h would pass through this coverage distance in three seconds, where the front transceiver completes the handover in the first second, communicate with base station in the following second, and perform the handover over to the next station in the last second, while the rear transceiver continues the communications with the last base station during this time.

A. Dual Wavelength Model

The received power on the covered distance along the track dictates the optimal longitudinal and lateral distances of the base station transceiver. Figure 4 shows the received power at the farthest point, D_i, along the track under consideration of heavy fog and geometrical losses. Note that the received power at D_i is the smallest one along the coverage distance. In this figure, the received power at point D_i is calculated as a function of the longitudinal distance, for a lateral distance between 0.25 to 2 m, with a step size of 0.25 m. The crosses on this graph indicate the points on the curves where the received power is the largest at D_i and determine the optimal longitudinal distance for a given lateral distance. Table III summarizes the optimal lateral and longitudinal distances. This figure shows that for a longitudinal distance around 500 m, the received power is the largest. Moreover, for a longitudinal distance smaller than 75 m, the received power is below the receiver sensitivity. The figure also shows that as the lateral distance decreases, the received power increases. Therefore, these results suggest placing the base stations as close to the track as possible.

TABLE III
Optimal Longitudinal Distances for Different Lateral Distances.

$\lvert B_iA_i\rvert$ (m)	$\lvert A_iC_i\rvert$ (m)	θ (°)	P_r at H_3 (dBm)	P_{rx} at D_i (dBm)
0.25	500.8	0.0153	-8.73	-17.42
0.50	508.2	0.0253	-20.64	-29.32
0.75	509.7	0.0332	-27.66	-36.34
1.00	510.2	0.0400	-32.64	-41.33
1.25	510.5	0.0448	-36.53	-45.20
1.50	510.6	0.0496	-39.68	-48.37
1.75	510.7	0.0536	-42.36	-51.04
2.00	510.8	0.0567	-44.68	-53.36

As Table III shows, there is an optimal longitudinal distance for each lateral distance. These results suggest a lateral distance smaller than 0.75 m and its corresponding optimal longitudinal distance to provide a received power large enough at the train transceivers in heavy-fog conditions.

Figure 5 shows the received power at D_i versus the longitudinal distance in clear weather conditions. This figure shows that for the same lateral and longitudinal distances, the received power in the DW model receives more power in clear weather than it does in heavy-fog conditions, as expected. As the longitudinal distance increases, the received power also increases because the divergence angle decreases, as described by (11). However, for the same system in heavy-fog conditions, we observe that for longitudinal distances beyond 509 m, the received power decreases, as Figure 4 shows.

B. Handover Time

We also analyzed the effect of the handover time over the received power at the transceivers. As the handover time decreases, the required coverage distance of the base stations in the DW model decreases. A reduction of the coverage distance leads to a decrease of the link range and therefore, the received power increases at D_i. Figure 6 shows the received

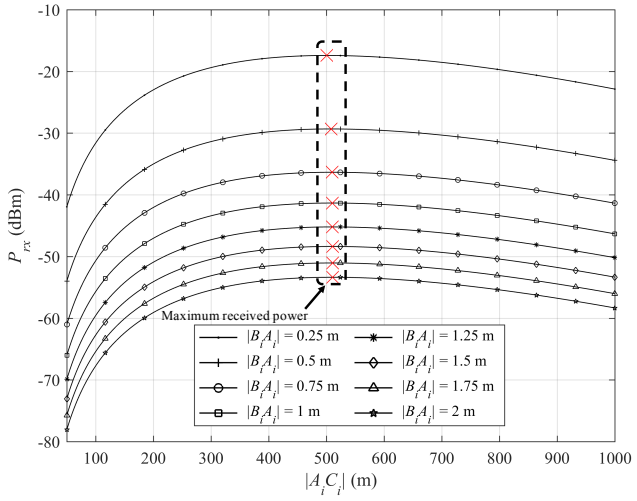

Fig. 4. Received power at D_i vs. longitudinal distance.

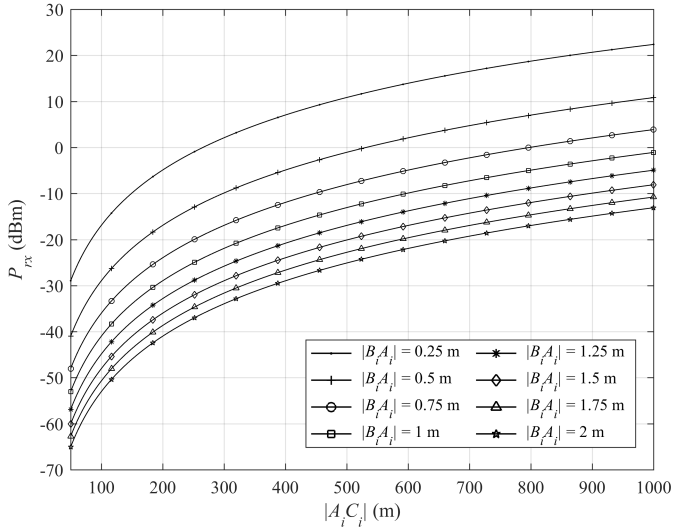

Fig. 5. Received power at D_i vs. longitudinal distance in clear weather conditions.

power at D_i versus the required coverage distance along the track. As Figure 6 shows, for a lateral distance up to 2 m and a coverage distance of about 165 m (or a handover time of 0.5 s to maintain the set duty cycle), the received power is larger than or equal to the receiver sensitivity. However, for a lateral distance greater than 2 m, a handover time smaller than 0.5 s (corresponding to a coverage distance shorter than 165 m for the set duty cycle) is required to achieve a seamless connection.

Figure 7 shows the received power at D_i versus the coverage distance. In clear weather conditions, with a visibility beyond 50 km, the received power is about 20 dB higher than in heavy-fog conditions at the same location on the track. This graph is plotted for a longitudinal distance of 509 m. As this figure shows, the smallest received power along the track is larger than the required receiver sensitivity for a lateral distance smaller than or equal to 4 m. Therefore, the DW model in

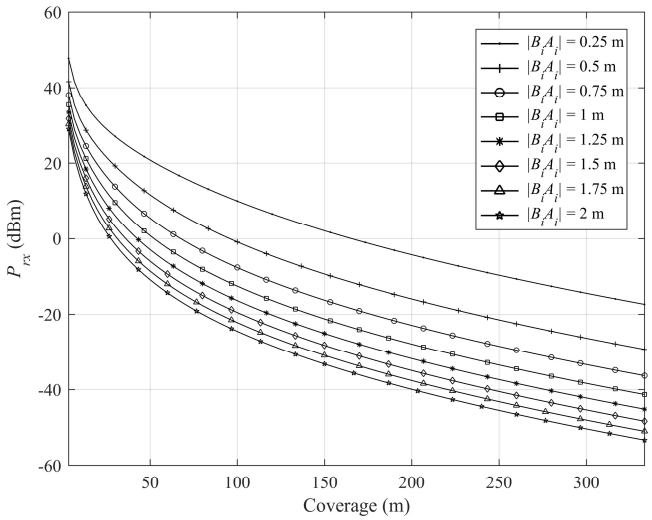

Fig. 6. Received power at D_i vs. coverage distance.

clear weather conditions may operate with a lateral distance larger than that in heavy-fog conditions for a given coverage distance.

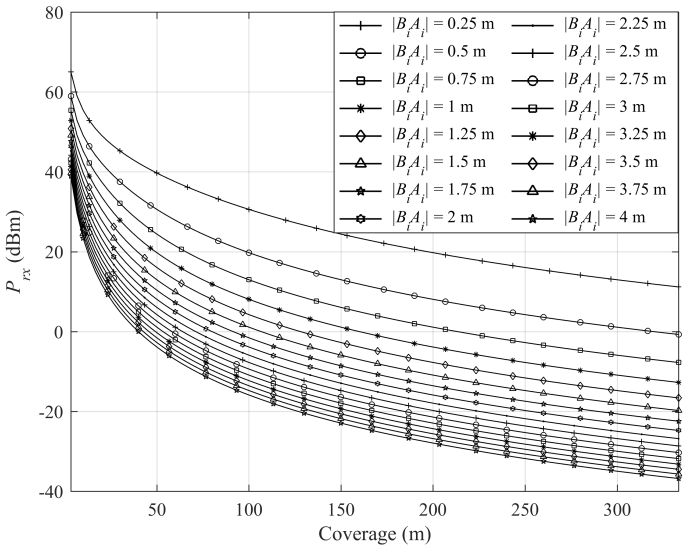

Fig. 7. Received power at D_i vs. coverage distance in clear weather.

Figure 8 shows the received power along the coverage distance of a base station for the optimal longitudinal and lateral distances. These calculations are based on (19). The location points marked with a red cross in each curve in this figure indicate the maximum received power along the track, which occurs at H_2. The received power decreases as we move away from H_2 to the boundaries of the coverage distance, because the beam offset is zero at H_2. However, at points C_i and D_i, the beam offset is equal to the beam radius, which leads to a smaller received power at those points. The minimum received power occurs at the farthest coverage point of a base station along the track. As shown in this

graph, for a lateral distance smaller than 0.75 m, and the optimal longitudinal distance as presented in Table III, the received power is larger than the receiver sensitivity for a data transmission bandwidth of 1.25 Gbps. However, for a lateral distance greater than or equal to 0.75 m, the power levels drop below the receiver sensitivity. In the DW model, the distance between two adjacent base stations is about 222 m, based on the target duty cycle.

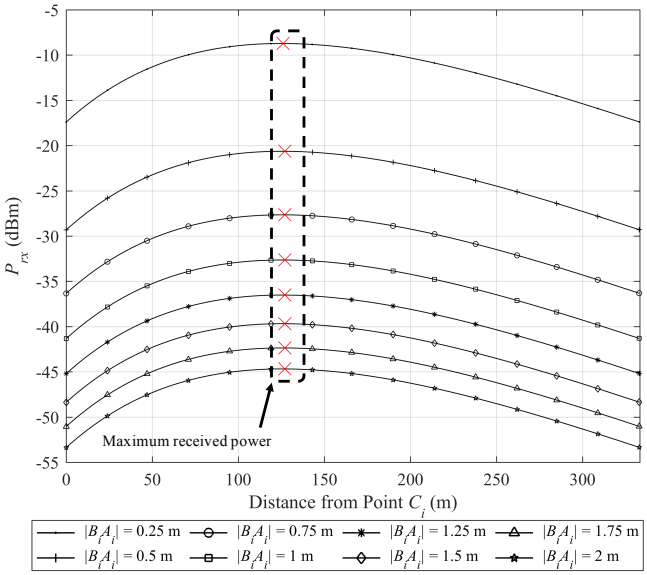

Fig. 8. Received power along track.

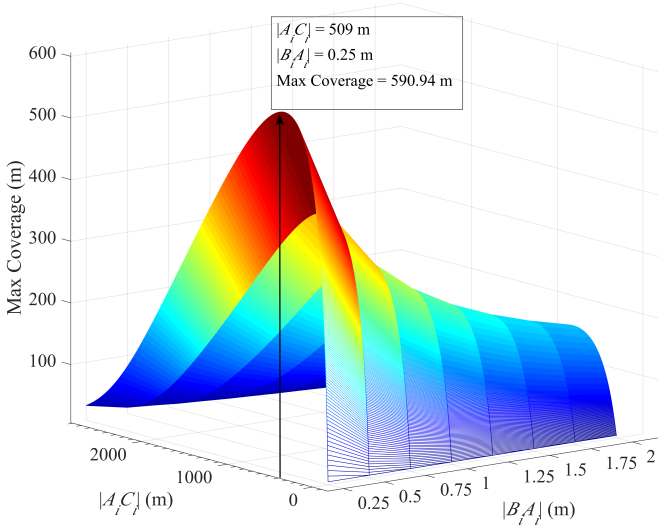

Fig. 9. Maximum achievable coverage distance vs. lateral and longitudinal distances.

C. Single Wavelength Model

In general, the analysis of the SW model is similar to that for the DW model, except for the additional distance of the dark region. The formulas and calculation of light dispersion and received power for the SW model are the same as those for the DW model. Therefore, calculations in Figures 4 to 8 also apply to the SW model. The main difference between these two models is the areas covered along the railroad and the conditions to trigger handovers. Figure 9 shows the maximum achievable coverage distance versus lateral and longitudinal distances that satisfy the receiver sensitivity. As this figure shows, by decreasing the lateral distance, the maximum achievable coverage distance increases. For a given longitudinal distance, the optimal lateral distance results in the maximum achievable coverage distance. For a lateral distance of 0.25 m and the optimal longitudinal distance equal to 509 m, the maximum achievable coverage distance is about 590 m. This maximum coverage is marked by a black arrow in Figure 9. For other longitudinal distances, the achievable coverage distance decreases.

So far, the results seem to indicate that the smaller the lateral distance is, the larger coverage and received power are attained. However, the cost of achieving these results depends on the divergence angle. As the lateral distance decreases, the required divergence angle for the system also decreases. Smaller divergence angles result in smaller geometrical losses and larger received power at train transceivers. For a lateral distance equal to 2 m and a longitudinal distance of 509 m, a transmitter with a divergence angle of about 0.059° is required. As this figure shows, for a very small lateral distance (e.g., 0.01 m), the required divergence angle would be very small.

V. Conclusions

In this paper, two free-space optical coverage models for high speed trains have been proposed; the single wavelength (SW) and the dual wavelength (DW) models. The DW model uses two different wavelengths for communications, where the wavelengths are alternated between adjacent base stations. The front transceiver performs the needed handover when the train moves from one area covered by a base station to another, while a rear train transceiver continues communicating with the last base station. These models are aimed at maximizing the laser-light coverage of portions of the track of a high-speed train to communicate through FSO links and to allocate enough time for performing handovers. We calculate the optimal distance of a base stations to the train track and the required distance between adjacent base stations, such that ground-to-train and train-to-ground attain 1 Gbps or higher and provide efficient coverage along the track. For a lateral distance in the range of 0.25 to 0.75m, the received power is larger than receiver sensitivity. For a lateral distance in this range, the optimal longitudinal distance is in the range of about 500 to 510 m. For a lateral distance of 0.25 m, the optimal longitudinal distance is calculated to be approximately 509 m. To ensure a wide data connection bandwidth, lateral distances of up to 0.75 m may be used. Because the railroad of HSTs is flat and the placement of the transceivers is very close to the track, no terrain obstacles nor vegetation are expected. Therefore, obstacles are not considered in the analysis except for

the weather conditions analyzed in this paper. Therefore, the numerical evaluations consider a heavy-fog condition as the worst-case scenario for FSO links. This base station position enables using appropriate distances between transceivers to overcome losses caused by heavy fog. Moreover, the distance between transceivers on the train must be large enough to accommodate the longest handover time and the length of the dark region in the SW model.

The calculation of received power based on the location of a base station and relative to rail track shows that a smaller lateral distance from the rail track provides a larger received power along the coverage distance.

REFERENCES

[1] Top ten fastest trains in the world. [Online]. Available: http://www.railway-technology.com/features/feature-top-ten-fastest-trains-in-the-world/

[2] Schwieterman, Schulz, Forst, Michel, and Sellers, "The digitally connected commuter: Tracking the rising use of personal electronic devices on chicago suburban trains," 2015.

[3] W. Luo, R. Zhang, and X. Fang, "A comp soft handover scheme for lte systems in high speed railway," *EURASIP Journal on Wireless Communications and Networking*, vol. 2012, no. 1, pp. 1–9, 2012.

[4] X. Qian, H. Wu, and J. Meng, "A dual-antenna and mobile relay station based handover in distributed antenna system for high-speed railway," in *Innovative Mobile and Internet Services in Ubiquitous Computing (IMIS), 2013 Seventh International Conference on*. IEEE, 2013, pp. 585–590.

[5] Q. Wang, G. Ren, and J. Tu, "A soft handover algorithm for td-lte system in high-speed railway scenario," in *Signal Processing, Communications and Computing (ICSPCC), 2011 IEEE International Conference on*. IEEE, 2011, pp. 1–4.

[6] R. K. Kalle, P. Angolkar, D. Das, and R. Ramalingam, "Swift: A novel architecture for seamless wireless internet for fast trains," in *Vehicular Technology Conference, 2008. VTC Spring 2008. IEEE*. IEEE, 2008, pp. 3011–3015.

[7] D. T. Fokum and V. S. Frost, "A survey on methods for broadband internet access on trains," *Communications Surveys & Tutorials, IEEE*, vol. 12, no. 2, pp. 171–185, 2010.

[8] Y. Zhou and B. Ai, "Handover schemes and algorithms of high-speed mobile environment: A survey," *Computer Communications*, vol. 47, pp. 1–15, 2014.

[9] O. B. Karimi, J. Liu, and C. Wang, "Seamless wireless connectivity for multimedia services in high speed trains," *Selected Areas in Communications, IEEE Journal on*, vol. 30, no. 4, pp. 729–739, 2012.

[10] B. Ai, X. Cheng, T. Kürner, Z.-D. Zhong, K. Guan, R.-S. He, L. Xiong, D. W. Matolak, D. G. Michelson, and C. Briso-Rodriguez, "Challenges toward wireless communications for high-speed railway," *IEEE Transactions on Intelligent Transportation Systems*, vol. 15, no. 5, pp. 2143–2158, 2014.

[11] L. Zhu, F. R. Yu, B. Ning, and T. Tang, "Cross-layer handoff design in mimo-enabled wlans for communication-based train control (cbtc) systems," *IEEE Journal on Selected Areas in Communications*, vol. 30, no. 4, pp. 719–728, 2012.

[12] IEEE802.11p/D3.0, "Draft amendment for wireless access in vehicular environments (wave)," 2007.

[13] O. Teyeb, V. Phan, B. Raaf, and S. Redana, "Handover framework for relay enhanced lte networks," in *2009 IEEE International Conference on Communications Workshops*. IEEE, 2009, pp. 1–5.

[14] "3gpp ts 23.009 version 13.0.0, handover procedures," *ETSI*, 2016.

[15] L. Tian, J. Li, Y. Huang, J. Shi, and J. Zhou, "Seamless dual-link handover scheme in broadband wireless communication systems for high-speed rail," *Selected Areas in Communications, IEEE Journal on*, vol. 30, no. 4, pp. 708–718, 2012.

[16] L. Tain, Y. Zhou, J. Li, Y. Huang, J. Shi, and J. Zhou, "A novel handover scheme for seamless wireless connectivity in high-speed rail," in *Wireless and Mobile Computing, Networking and Communications (WiMob), 2011 IEEE 7th International Conference on*. IEEE, 2011, pp. 230–236.

[17] I. Ahmad and D. Habibi, "A novel mobile wimax solution for higher throughput," in *Networks, 2008. ICON 2008. 16th IEEE International Conference on*. IEEE, 2008, pp. 1–5.

[18] K. Guan, G. Li, T. Kuerner, A. F. Molisch, B. Peng, R. He, B. Hui, J. Kim, and Z. Zhong, "On millimeter wave and thz mobile radio channel for smart rail mobility," *IEEE Transactions on Vehicular Technology*, vol. PP, no. 99, pp. 1–1, 2016.

[19] Internet connection speed recommendations. [Online]. Available: https://help.netflix.com/en/node/306

[20] B. Ai, K. Guan, M. Rupp, T. Kurner, X. Cheng, X.-F. Yin, Q. Wang, G.-Y. Ma, Y. Li, L. Xiong *et al.*, "Future railway services-oriented mobile communications network," *IEEE Communications Magazine*, vol. 53, no. 10, pp. 78–85, 2015.

[21] Sonabeam 2500-z. [Online]. Available: http://www.fsona.com/product.php?sec=2500z

[22] Aire x-stream fso. [Online]. Available: http://www.lightpointe.com/aire-x-stream-fso–ultra-low-latency-.html

[23] A. K. Majumdar and J. C. Ricklin, *Free-space laser communications: principles and advances*. Springer Science & Business Media, 2010, vol. 2.

[24] H. Urabe, S. Haruyama, T. Shogenji, S. Ishikawa, M. Hiruta, F. Teraoka, T. Arita, H. Matsubara, and S. Nakagawa, "High data rate ground-to-train free-space optical communication system," *Optical Engineering*, vol. 51, no. 3, pp. 031 204–1, 2012.

[25] K. Mori, M. Terada, K. Nakamura, R. Murakami, K. Kaneko, F. Teraoka, D. Yamaguchi, and S. Haruyama, "Fast handover mechanism for high data rate ground-to-train free-space optical communication system," in *Globecom Workshops (GC Wkshps), 2014*. IEEE, 2014, pp. 499–504.

[26] R. Paudel, Z. Ghassemlooy, H. Le-Minh, and S. Rajbhandari, "Modelling of free space optical link for ground-to-train communications using a gaussian source," *Optoelectronics, IET*, vol. 7, no. 1, pp. 1–8, 2013.

[27] R. Paudel, J. Poliak, Z. Ghassemlooy, and E. Leitgeb, "Modelling and analysis of fso ground-to-train communications for straight and curved tracks," in *Antennas and Propagation (EuCAP), 2013 7th European Conference on*. IEEE, 2013, pp. 3180–3184.

[28] X. Yin, X. Cai, X. Cheng, J. Chen, and M. Tian, "Empirical geometry-based random-cluster model for high-speed-train channels in umts networks," *IEEE Transactions on Intelligent Transportation Systems*, vol. 16, no. 5, pp. 2850–2861, 2015.

[29] X. Cheng, C.-X. Wang, B. Ai, and H. Aggoune, "Envelope level crossing rate and average fade duration of nonisotropic vehicle-to-vehicle ricean fading channels," *IEEE Transactions on Intelligent Transportation Systems*, vol. 15, no. 1, pp. 62–72, 2014.

[30] X. Cheng, Q. Yao, M. Wen, C.-X. Wang, L.-Y. Song, and B.-L. Jiao, "Wideband channel modeling and intercarrier interference cancellation for vehicle-to-vehicle communication systems," *IEEE Journal on Selected Areas in Communications*, vol. 31, no. 9, pp. 434–448, 2013.

[31] T. Arita and F. Teraoka, "Providing a high-speed train with a broadband nemo environment: a report of a field test using a train in service," in *Proceedings of the Sixth Asian Internet Engineering Conference*. ACM, 2010, pp. 64–71.

[32] P. F. Goldsmith, I. of Electrical, E. Engineers, M. Theory, and T. Society, *Quasioptical systems: Gaussian beam quasioptical propagation and applications*. IEEE press New York, 1998.

[33] O. Svelto, *Principles of lasers*. Springer Science & Business Media, 2010.

[34] X. Liu, "Free-space optics optimization models for building sway and atmospheric interference using variable wavelength," *Communications, IEEE Transactions on*, vol. 57, no. 2, pp. 492–498, 2009.

[35] S. G. Lambert and W. L. Casey, *Laser communications in space*. Artech House, 1995.

[36] H. Henniger and O. Wilfert, "An introduction to free-space optical communications," *Radioengineering*, vol. 19, no. 2, pp. 203–212, 2010.

[37] J. Akella, C. Liu, D. Partyka, M. Yuksel, S. Kalyanaraman, and P. Dutta, "Building blocks for mobile free-space-optical networks," in *Wireless and Optical Communications Networks, 2005. WOCN 2005. Second IFIP International Conference on*. IEEE, 2005, pp. 164–168.

[38] P. W. Kruse, L. D. McGlauchlin, and R. B. McQuistan, "Elements of infrared technology: generation, transmission and detection," *New York: Wiley, 1962*, 1962.

[39] D. Swinehart, "The beer-lambert law," *J. Chem. Educ*, vol. 39, no. 7, p. 333, 1962.

[40] I. I. Kim, B. McArthur, and E. Korevaar, "Comparison of laser beam propagation at 785 nm and 1550 nm in fog and haze for optical wireless communications," in *proc. SPIE*, vol. 4214, 2001, pp. 26–37.

[41] V. Arya, "Analysis, design and performance evaluation of optical fiber spectrum-sliced wdm systems," 1997.

[42] S. Bloom, E. Korevaar, J. Schuster, and H. Willebrand, "Understanding the performance of free-space optics [invited]," *Journal of optical Networking*, vol. 2, no. 6, pp. 178–200, 2003.